Preparation and properties of composite oxide hydrogen blocking coatings by sintering method

Abstract: The α-Al_2O_3/Cr_2O_3/SiO_2 composite coating was prepared on a 316L stainless steel sheet using ceramic sintering. The effect of sintering temperature on the coating was studied, and the coating's microstructure, structure, and properties were observed. The main research results are as follows: When sintering at 725℃ and slurry ratio is 1:5, the coating surface is smooth, no holes and cracks occur, the coating morphology is uniform, and the average thickness is about 64μm. The microstructure analysis showed that Cr_2O_3 and SiO_2 were uniformly distributed in the coating, Al_2O_3 segregation existed outside the coating, and a new phase of Al_2SiO_5 was produced. The composite coating with a slurry ratio 1:5 has the best hydrogen and thermal shock resistance, and its permeability reduction factor is 15.31 compared with 316L. It can withstand 20 thermal cycles at 450℃.

Keywords: Hydrogen blocking coating; 316L stainless steel; Ceramic sintering method; Hydrogen blocking performance

1. Introduction

As a green and clean secondary energy source, hydrogen energy will play an essential role in the future global energy system[1]. Hydrogen transportation mainly adopts high-pressure gas, low-temperature liquid, and pipeline transportation. Due to the small volume of hydrogen atoms, it is easy to penetrate the metal under a high-pressure environment and cause the deterioration of material properties, such as hydrogen damage, hydrogen brittleness, and other performance problems, which may lead to severe production safety accidents and economic losses. Therefore, the hydrogen energy industry urgently needs to solve the safety problems in the storage and transportation of hydrogen[2,3].

To slow down the penetration and diffusion of hydrogen in metal structural materials, the preparation of hydrogen-blocking coatings was an effective means to prevent or delay the penetration of hydrogen into the material and prevent the occurrence of hydrogen embrittle[4-6]. Traditional ceramic hydrogen blocking coatings can be divided into non-oxide coatings and oxide coatings, such as titanium ceramics such as TiC, TiN and TiAlN, silicide ceramics such as SiC and Si_3N_4, oxidesceramicsuch as Al_2O_3, Cr_2O_3, Er_2O_3, SiO_2 and TiO_2, etc.[7-10]. Compared with silicides, carbides and other coatings, oxide coatings have the advantages of good high temperature

resistance and chemical stability, can effectively prevent the penetration of hydrogen, improve the corrosion resistance and safety of metal materials. In particular, Al_2O_3 coating, as a hydrogen resistant coating, has excellent hydrogen resistance and chemical stability, and can effectively protect the metal matrix from the influence of hydrogen embrittlement and corrosion. However, Al_2O_3 coating also has some problems, such as low bonding strength and easy peeling. To solve this problem, Al_2O_3 is generally mixed with gas oxides to make composite coatings [11,12]. The thermal expansion coefficient of Cr_2O_3 is not much different from that of stainless steel, and the binding force of Cr_2O_3 coating is better. It also has excellent hydrogen resistance and chemical stability[13] . However, the coatings fired by these two composite materials have no ceramic luster and poor topography. At the same time, the addition of SiO_2 can be used as the glaze of the ceramic coating to improve the coating topography, and the addition of SiO_2 can optimize the microstructure of the coating and adjust the physical properties of the coating [14,15].

Therefore, α-Al_2O_3, Cr_2O_3, and SiO_2 are mixed in a particular proportion to make a powder, and a certain amount of binder is expected to have a dense structure and uniform organization of hydrogen-blocking coating. In this paper, α-Al_2O_3/Cr_2O_3/SiO_2 composite oxide hydrogen blocking coating was prepared by optimizing the sintering temperature and slurry ratio. The coating's morphology, microstructure, and phase composition were analyzed, and the thermal shock and hydrogen-blocking performance were tested.

2. Experimental materials and methods

Round sheet 316L stainless steel with a diameter of 32mm and thickness of 2mm was used as the base material of the hydrogen resistance coating. In turn, 400#-1000# SiC sandpaper was used to polish the stainless steel surface. The sample is then cleaned in alcohol using ultrasonic waves. Finally, the treated sample was placed in the oven at 50℃ for drying.

The ratio of powder raw materials was α-Al_2O_3: Cr_2O_3: SiO_2= 1:1:2:6 ratio of coating, using a planetary ball mill for 2 h grinding. After that, the powder was mixed with the inorganic silicone adhesive at a ratio of 1:5, and the evenly dispersed slurry was obtained by mechanical stirring for 1h. The slurry was coated on a stainless steel matrix using the spinning coating method and then sintered in a muffle furnace at different temperatures after natural drying for 24 h. The sintering heating rate was 2℃/min.

X-ray diffractometer model DX-2700BHX was used for coating phase analysis. The test Angle was 10-90°, the scanning speed was 6°/min, the tube voltage was 40kV, and the tube current was 30mA. Scanning electron microscopy (SEM) model TESCANVEGA3-LMU and its equipped energy spectrometer were used to observe the morphology and composition of the coating surface and cross-section.

The electrochemical hydrogen penetration method was used to test the hydrogen inhibition performance of the coating [16]. The basic principle was to evaluate the barrier effect of the coating on hydrogen diffusion by constructing a two-part system consisting of a cathode pool and an anode pool. NaOH solution was used as the electrolyte in the anode chamber, and the electrolyte in the cathode chamber was a mixed solution of NaOH and thiourea. The specimen was plated with nickel to prevent the diffused hydrogen from recombining into hydrogen molecules. The specimen clamp was placed in the system to ensure the nickel-coated surface faced the anode side. Then, the delay time method [16] was used to calculate the hydrogen permeability coefficient of the sample:

$$\mathrm{D} = \frac{L^2}{6t_L} \quad (1)$$

Where D is the apparent hydrogen permeability coefficient, L is the thickness of the sample used, and the hydrogen permeation current is the time minus the time when the hydrogen permeation experiment began. The hydrogen permeability reduction factor PRF was calculated by comparing the permeability coefficient of H ion in the downstream chamber between the uncoated stainless steel matrix and the coated stainless steel sample.

A static thermal shock test was adopted, and the sample was put into the Muffle furnace, held for 450 minutes, and then quenched to observe the morphology changes of the coating and the thermal shock resistance of the coating. The above experiment was repeated until the coating fell off, and the number of thermal shocks was counted.

3. Experimental results and analysis

3.1 Coating phase composition

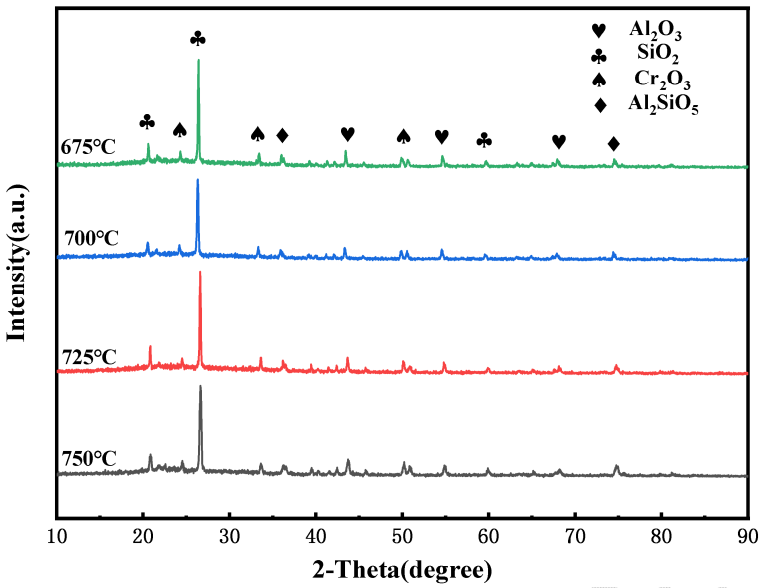

Fig. 1 X-ray diffraction patterns of composite coatings at different sintering temperatures

Fig. 1 shows the XRD pattern of the coating sintered at different temperatures. It can be seen that under the sintering at the above four temperatures, the coating phase was the same, the α-Al_2O_3phase, the Cr_2O_3 phase, the SiO_2 phase, and the Al_2SiO_5 phase, and no new phase was produced. Under the conditions of the temperature and slurry ratio, the main phases of the coating were the α-Al_2O_3 phase, Cr_2O_3 phase, SiO_2 phase, and Al_2SiO_5 phase, among which the α-Al_2O_3 phase, Cr_2O_3 phase, and SiO_2 phase were mainly from the added oxide powder. Al2SiO5 was a new phase precipitated by the reaction of the α-Al_2O_3 phase and SiO_2 phase at high temperatures [17].

3.2 Coating Morphology

Fig. 2 shows the macroscopic morphology of the composite coating prepared by sintering. As can be seen from the figure, when the sintering temperature was 675℃, there were many large holes on the surface of the coating, exposing the stainless steel matrix, and the coating was matte. When the temperature increased to 700℃, the number of holes decreased, the area also decreased, only scattered small holes formed, and the coating surface was smooth. When the temperature was increased to 725℃, the number of holes reached the minimum, the coating surface was smooth, and the coating morphology was best. When the temperature rose to 750 ° C, the coating surface began forming a larger area of holes, a small part of the stainless steel matrix was exposed, and the coating quality decreased. By comparing the surface morphology of the coating at several temperatures, it is found that the best

morphology of the coating was sintered at 725℃, so the sintering temperature of the coating is determined to be 725℃.

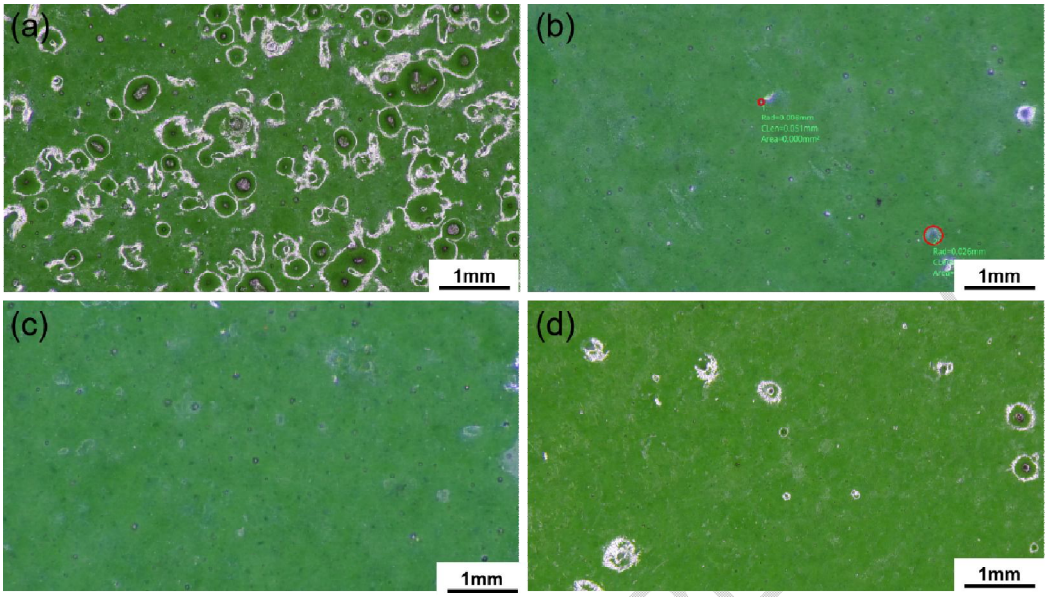

Fig. 2 Macroscopic morphology of sintered coatings at different temperatures: (a)675℃; (b)700 ° C; (c)725 ° C; (d)750℃

The best morphology of composite coating was prepared when the slurry ratio was 1:5, and the sintering temperature was 725℃. To study the microstructure of the coating further, scanning electron microscopy was used to observe the surface and cross-section of the coating. Fig. 3 shows the surface topography of α-$Al_2O_3/Cr_2O_3/SiO_2$ composite coating at different magnifications. In general, the coating surface was relatively flat, and there were no holes, cracks, or other defects. However, the selected oxide particle size was different; the oxide particles were agglomerated, and the coating surface had a slight fluctuation of pits and particles.

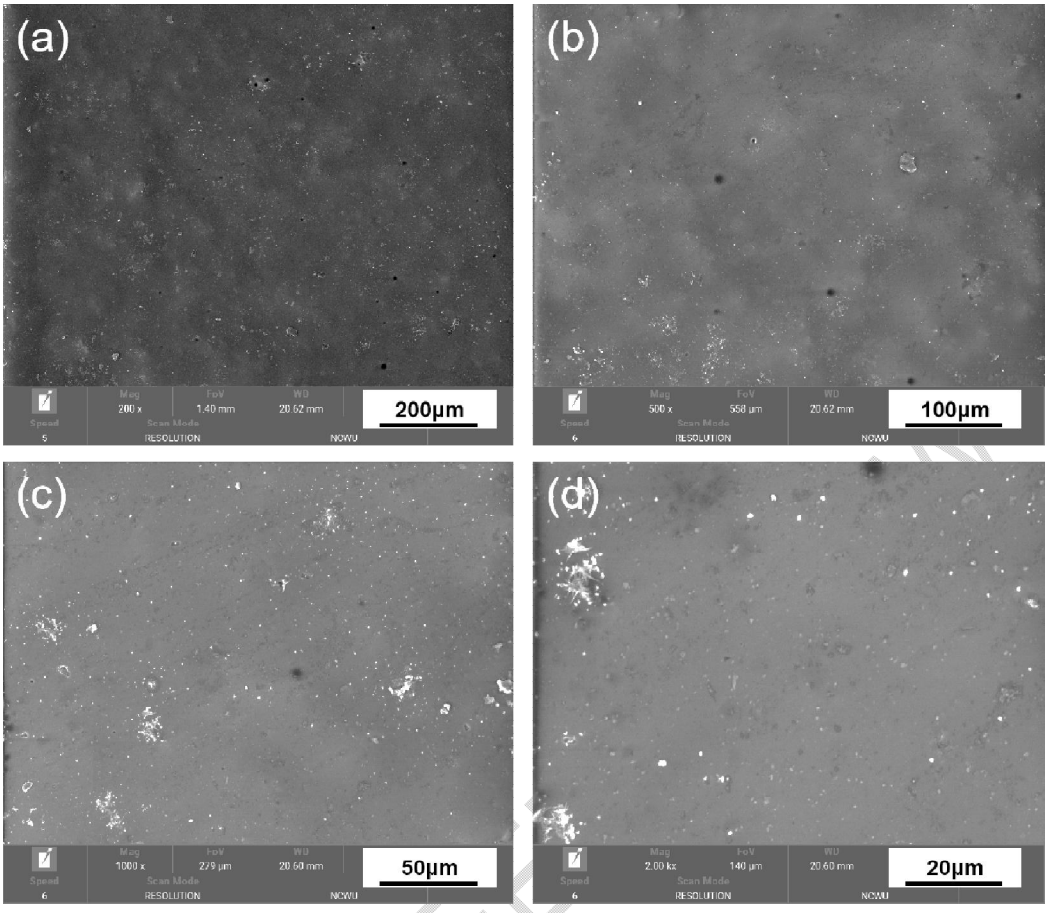

Fig. 3 Surface topography at different magnifications: (a)200x; (b)500x; (c)1000x; (d)2000x

Fig. 4 shows the cross-section topography of the coating. It can be measured from the figure that the average thickness of the coating was 64µm, and there were about 15µm holes in the coating. This was because the oxide particle size of the coating preparation was different; the different particles were stacked together, and there were specific pores, inorganic silica gel adhesive as a liquid phase, filled in these pores so that the particles were combined. Still, carbon and other elements were in the inorganic silica gel adhesive; the temperature rose, the elements were oxidized, and other gases, such as CO_2, were generated. When the temperature reached the glass transition temperature (Tg), the components were transformed into the liquid phase. Still, the coating surface was sintered faster and became dense, preventing the gas inside the coating from being discharged, resulting in some gas remaining inside the coating. After the sintering was completed, the undischarged gas formed holes. Although there are holes in the coating, they do not penetrate the entire coating, and no cracks are created around them, reducing the risk that these holes will cause the

coating to crack and fall off.

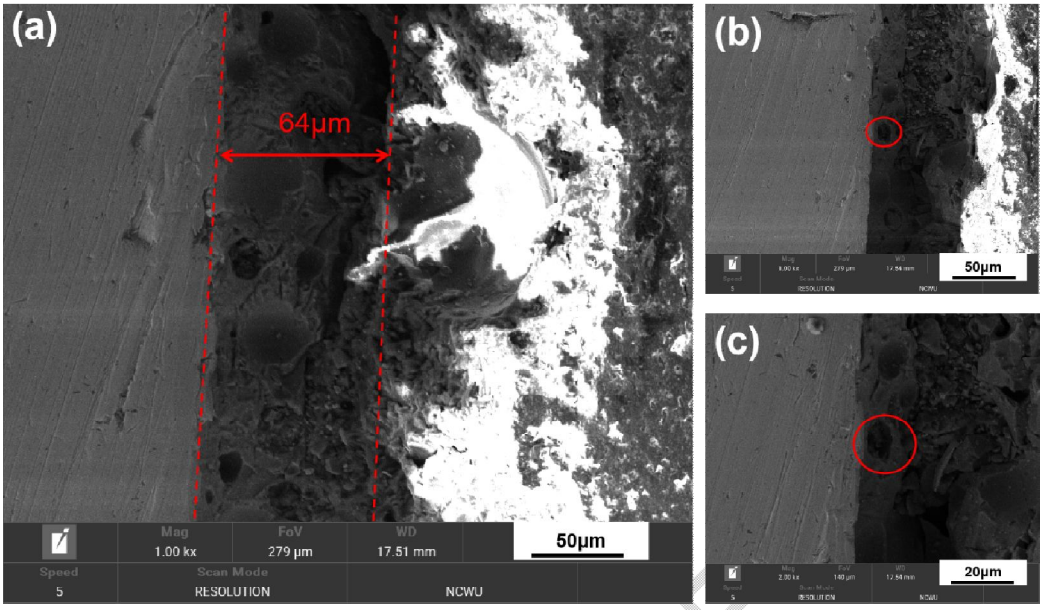

Fig. 4 Coating thickness diagram and cross-section topography of different magnifications, (a) coating thickness diagram, (b)1000×, (c)2000×

3.3 Hydrogen resistance performance

Fig. 5 shows the hydrogen resistance curves of the stainless steel matrix and composite coating at room temperature. According to formula (1), the PRF of the stainless steel matrix and composite coating were calculated to be 1 and 15.3, respectively. One of the reasons for the excellent hydrogen resistance of the coating was the formation of the Al_2SiO_5 crystal structure during the high-temperature sintering process. This crystal structure has high density and stability, making the coating atoms more tightly packed and forming a dense lattice structure with good hydrogen resistance. Secondly, EDS results showed that a large amount of α-Al_2O_3 and Cr_2O_3 were enriched on the surface of the coating. These two oxides have high electronegativity and strong interaction force with oxygen molecules, thus forming a dense oxide film on the surface of the coating. In addition, inorganic silica gel was used as an adhesive, SiO_2 was used as a ceramic sinter, and its molecular structure contained a large number of silicon-oxygen bonds, which made a dense layer of silica compounds formed on the surface of the coating, and the hydrogen channel in the coating became smaller, thus further enhancing the hydrogen resistance of the coating.

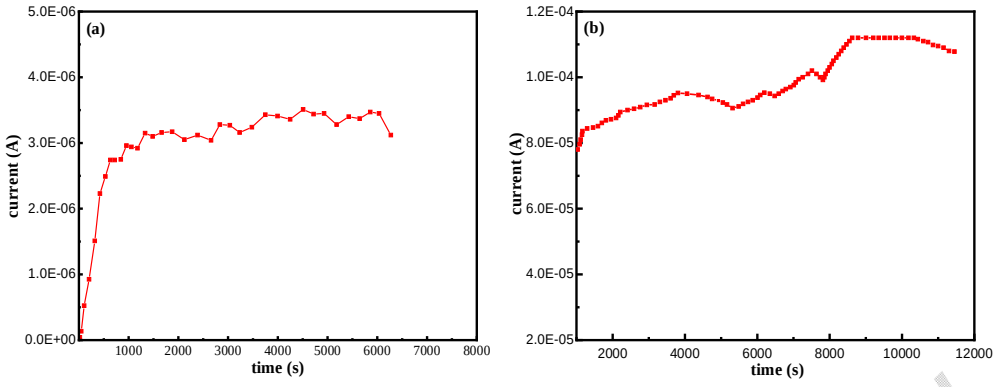

Fig. 5 Hydrogen permeation curves of 316L substrate and coating, (a) substrate, (b) Composite coating

3.4 Thermal shock resistance

Fig.6 shows the coating morphology with a slurry ratio 1:5 before and after thermal shock at 450℃. After 5 thermal shocks, the morphology of the coating did not change. After 20 thermal shocks, a large number of black spots and holes appeared in the coating, and the surface topography of the coating became worse, indicating that with the increase in the number of thermal shocks, the coating structure began to be damaged. These defects would become channels for hydrogen penetration. After 25 thermal shocks, the black spots in the coating expanded greatly, and the holes became larger; the stainless steel matrix was exposed, the direct contact between the matrix and the external environment could no longer be effectively isolated, and the hydrogen resistance of the coating was completely lost.

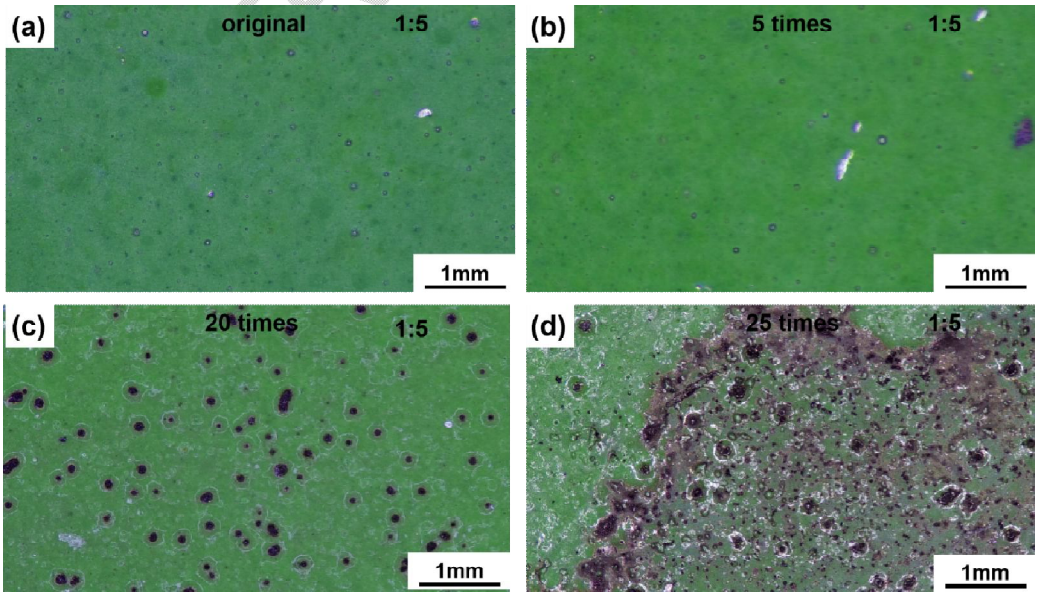

Fig. 6 Slurry ratio is the topography of the coating undergoing different thermal shock

times, (a) original, (b) 5times, (c) 20 times, (d) 25times

4. Conclusion

When the heating rate was 2℃/min, the sintering temperature was 725℃, the slurry ratio was 1:5, the coating surface was smooth and uniform, and the coating morphology was the best. There was α-Al_2O_3 polarization on the outside of the coating, Cr_2O_3 was evenly distributed in the coating, and the chemical reaction of the coating produced an Al_2SiO_5 phase during the sintering process. The hydrogen resistance test showed that the PRF of the coating reached 15.31, and the number of thermal shocks when the coating cracks was 20 times.

Reference

[1] Le P A, Trung V D, Nguyen P L, et al. The current status of hydrogen energy: an overview, RSC advances, 2023, 13(40): 28262-28287.

[2] Gao Hui, Yang Yan, Zhao Xu, et al. Current situation and thinking of hydrogen energy industry development at home and abroad, International Petroleum Economics,2019,27(04):9-17.

[3] Mueller K, Arlt W, Status and Development in Hydrogen Transport and Storage for Energy Applications, Energy Technology, 2013, 1(9):501-511.

[4] Yang N, Deng J, Wang C, et al. High pressure hydrogen leakage diffusion: Research progress, International Journal of Hydrogen Energy, 2023.

[5] He D, Lei Y, Zhang C, et al. Deuterium permeation of Al_2O_3/Cr_2O_3 composite film on 316L stainless steel, International Journal of Hydrogen Energy, 2015, 40: 2899-2903.

[6] Dharamshi HK, Bhadeshia H, Prevention of Hydrogen Embrittlement in Steels, ISIJ INTERNATIONAL, 2016, 56: 24-36.

[7] Zhou QY, Lu ZX, Ling YH, et al. Characteristic and behavior of an electrodeposited chromium (III) oxide/silicon carbide composite coating under hydrogen plasma environment, Fusion Engineeringand Design, 2019, 143:137-146

[8] Tamura M, Eguchi T, Nanostructured thin films for hydrogen-permeation barrier, Journal of Vacuum Science& Technology A, 2015, 33: 041503.

[9] Zhu L, Zheng L, Xie H, et al. Design and properties of FeAl/Al2O3/TiO2 composite tritium-resistant coating prepared through pack cementation and sol-gel method, Materials Today Communications, 2020, 26:101848.

[10] Zheng ZY, Yang ZC, Yan YW,Effects of Internal Stress and Hydrogen Penetration on the Performance of Er_2O_3 Coatings as Hydrogen Permeation Barriers, ACS Applied Materials &Interfaces, 2024, 16: 22471-22481

[11] Fowler JD, Chandra D, Elleman TS, et al. Tritium diffusion in Al2O3 and BeO, Journal of the American Ceramic Society, 2007, 60(3- 4): 155-161.

[12] ZHANG T, Zhang Y Q, Wang J Nong, et al. Preparation and hydrogen resistance of 316L stainless steel surface oxide composite coating, Journal of Guangzhou University (Natural Science Edition),2023,22(06):69-76.

[13] Li Y, Barzagli F, Liu P, et al. Mechanism and Evaluation of Hydrogen Permeation Barriers: A Critical Review, Industrial & Engineering Chemistry Research, 2023, 62(39): 15752-15773.

[14] Zhou Chiliou, He Mohan, Xiao Shu, et al. Research progress of hydrogen resistance coating on stainless steel surface, Chemical Industry Progress,2020,39(09):3458-3468.

[15] Liu DG, Yang TT,Liu YL, et al. Thermal shock and tritium resistance of SiO2 coating on the inner wall of 316L stainless steel pipeline, Vacuum, 2021, 185:110032.

[16] Huang Kezhi. Preparation and hydrogen inhibition mechanism of APTES-GO modified epoxy resin /PVDF organic coating, Beijing General Research Institute of Nonferrous Metals,2024.

[17] Li Junjun, Wang Yunfeng, Zhang Aiju, et al. Effect of metallic aluminum powder and nano-Al_2O_3 powder on the properties of ceramic bond, Chinese Journal of Ceramics, 21,40(11):3777-3783